analytical chemistry

Article

pubs.acs.org/ac

Detection of H_2O_2 at the Nanomolar Level by Electrode Modified with Ultrathin AuCu Nanowires

Ning Wang,[†,∥] Yu Han,[†] Ying Xu,[†] Caizhen Gao,[†] and Xia Cao*[,‡,§]

[†]Key Laboratory of Bio-Inspired Smart Interfacia Science and Technology of Ministry of Education, School of Chemistry and Environment, Beijing University of Aeronautics and Astronautics, Beijing, 100083, China

[‡]School of Biochemical and Pharmaceutical Sciences, Capital Medical University, Beijing, 100069, China

[§]Beijing Institute of Nanoenergy and Nanosystems, Chinese Academy of Science, Beijing, 100083, China

[∥]Department of Chemistry, Dongguk University, Seoul 100-715, Korea

Supporting Information

ABSTRACT: Bimetallic AuCu nanowires (AuCuNWs) are synthesized via a facile water solution method at room temperature. Enhanced electrocatalytic activity is observed toward the oxidation of H_2O_2, which makes the AuCu nanowire, along with its unique catalytic properties, intriguing bifunctional mechanism, and surface atomic construction, a promising platform for the amplification of interfacing signal. A highly sensitive H_2O_2 biosensor is thus developed on the base of the as-prepared AuCuNW catalyst. A very low real determination limit (2.0 nM) was reached, and a linear range as wide as 5 orders of magnitude was demonstrated. In addition, a trace amount of H_2O_2, which was released from Raw 264.7 cells, was selectively detected, hinting at the possible applications for real-time quantitative detection of H_2O_2 in a biological environment.

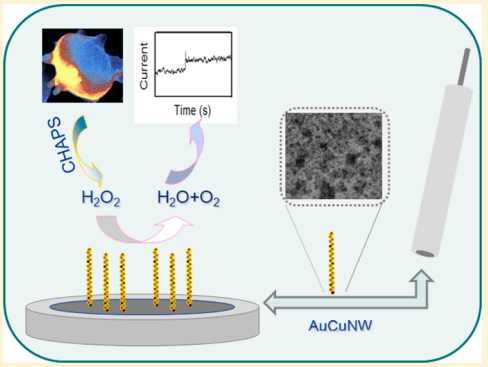

H_2O_2 is produced by most oxides and can exist in different biotissue compartments by penetrating freely through membranes.[1] Keeping H_2O_2 at an accessible level is very important for the robust operation of various cell functions.[2] Therefore, highly sensitive determination of H_2O_2 is necessary and vital in a wide variety of fields, from bioanalysis, to pharmaceutical security, to environmental protection.[3]

Until now, various H_2O_2 physicochemical sensing strategies have been developed and extensively studied.[4−7] In comparison with other techniques, the electrochemical methods make great progress because of their intrinsic merits, such as the low detection limit, sound reliability, good selectivity, and simple apparatus. These characteristics provide the accessibility to perform the quick detection of different analytes, even directly within the biological specimens in real-time mode.[8]

At present, to obtain a sound detection limit toward H_2O_2 for practical applications, electrochemical sensors are generally developed on the base of enzymes.[9] Unfortunately, both the biologic macromolecules and the as-fabricated sensors are generally lacking long-term stability, simply because of the loss of their biological functions caused by denaturation.[10] As a result, enormous research effort has been paid on developing advanced nonenzymatic sensing materials with enhanced enzyme−mimetic catalytic activity for H_2O_2 detection.[11]

Au-based bimetallic nanomaterials are drawing significant attention, because of their superior catalytic activity, in comparison with their single-phase counterparts.[11] For example, the electron coupling between the negatively charged top (vertex or corner) Au atoms with the Pd substrates resulted in a high activity toward the oxidation of glucose,[11g] while sound electrocatalytic activity toward methanol oxidation was demonstrated by the highly branched concave Au/Pd bimetallic nanocrystals.[11h] The composition- and shape-dependent properties of such bimetal nanocrystals have stimulated research into various synthetic strategies for highly efficient multidimensional design.[12] Previously, it has been proven that, besides the distinct synergetic effect caused by the surface strain and electronic coupling between the different components, the alloyed noble metals also present individual properties when used as electrocatalysts for electrochemical sensors. For example, while one metal such as Au in the alloy markedly lowers the activation energy, the other element within the alloy may help to provide abundant active sites, offer necessary biocompatibility, and/or improve the long-term stability.[12a,b] As a result, these nanoalloy-based electrodes provide access to rapid response, good stability, and high catalytic efficiency toward the targeted species.[12c−e,13] One-dimensional bimetallic nanowires are of particular interest, because they can offer much higher electrical conductivity and thus improved activity, relative to dispersed nanoparticles.[9c,14]

In this paper, AuCu nanowires were prepared via a mild single-step solution procedure. In this process, the formation of

Received: July 19, 2014
Accepted: November 24, 2014

   dx.doi.org/10.1021/ac502682n | *Anal. Chem.* XXXX, XXX, XXX−XXX

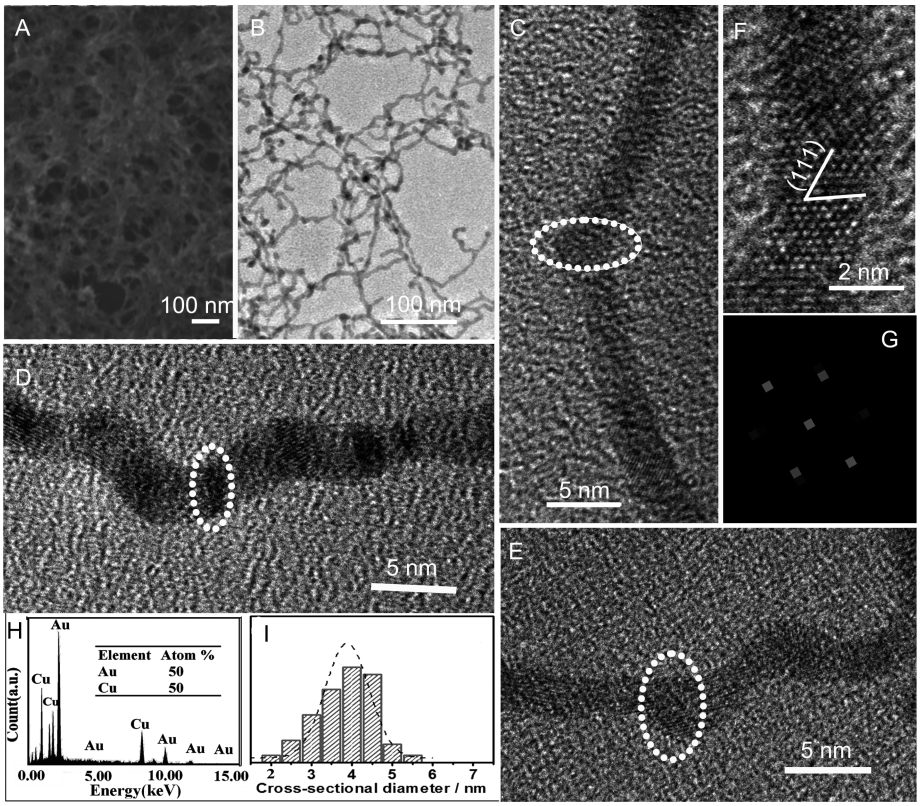

Figure 1. (A) Scanning electron microscopy (SEM) image, (C−E) transmission electron microscopy (TEM) images, and (F) HRTEM image of the AuCu nanowires with an average diameter of ∼4 nm. Also shown are (G) the fast Fourier transform (FFT) pattern, (H) the energy-dispersive spectroscopy (EDS) spectrum, and (I) the size distribution of the AuCu nanowires.

a precursory nucleus, crystal assembly, and one-dimensional growth can be observed sequentially. The as-produced AuCu nanowires have been explored as the modifying layer. Amperometric responses show that the AuCu nanowire, based on the glassy carbon electrode (GCE), gives sound sensitivity and selectivity toward the detection of H_2O_2. The good sensor performance should be ascribed to the as-expected synergetic effect that resulted from the coupling of Cu and Au atoms, which is especially so on the $Au_{67}Cu_{33}$ electrode. The detection of trace concentration of H_2O_2 released by cells has also been successfully achieved in this platform, which makes the (quasi-) one-dimensional nanoalloys very intriguing for use in direct real-time biosensing.

EXPERIMENTAL SECTION

Chemicals. All reagents, unless otherwise stated, were purchase from Sinopharm Chemical Reagent Beijing Co., Ltd., and used as received without further purification. Deionized water from a Milli-Q system was used throughout the experiments.

Synthesis of AuCu Nanowires. Typically, 40 mL of 5 mM $HAuCl_4{\cdot}3H_2O$, 40 mL of 5 mM of $CuCl_2{\cdot}2H_2O$, 0.001 g of sodium citrate, and 0.003 g of Triton-100 (dissolved in 10 mL of water), along with 20 mL of freshly prepared 60 mM $NaBH_4$ solution, were mixed together, sequentially, at room temperature under magnetic stirring within 2 min. After being maintained (without any further stirring) for 60 min at room temperature, the black powders were gathered by centrifuge and alternately washed by ethanol and pure water. To avoid any possible oxidation, all the steps of the synthesis were conducted under argon. The formation of nanowires occurs quickly, and the precipitation of a black solid can be observed within several minutes in the presence of $NaBH_4$. Au nanowires were synthesized for comparison. The synthetic process is very similar to that of the alloy. The only difference is the absence of a copper precursor. The atomic ratio of the AuCu nanowire was tuned by dealloying the nanoalloy with diluted HNO_3 (1:4 aqueous HNO_3 solution, v/v).

Fabrication of AuCu Nanowire-Modified Electrodes. In a typical electrode modifying process, 5 μL of 5 mg/mL AuCu nanowire (suspended in ethanol) was added onto the GCE surface (d = 3 mm) and dried in air to form a porous nanoalloy layer. To entrapping the AuCu nanowires, 5 μL of Nafion solution (1 wt % in ethanol) was then deposited dropwise onto the electrode surface to form a dense layer, which was then fully wetted by soaking the electrodes (denoted as Au_xCu_{100-x}NWE) in water for 1 h before use. Furthermore, Au wires (Au) and Au nanowire electrodes were also fabricated via the same process for further electrochemical comparison.

Apparatus and Electrochemical Measurements. Scanning electron microscopy (SEM) images were obtained, using a Hitachi Model S4800 cold field-emission scanning electron microscopy (CFE-SEM) system. Transmission electron microscopy (TEM) and high-resolution transmission electron microscopy (HRTEM) images were taken from a JEOL Model JEM-2100F TEM at 200 kV. To prepare the TEM samples, 2 μL of the powder/ethanol suspension was added onto a carbon-coated Ni grid and dried in air. Elemental composition was characterized using the energy-dispersive X-ray analysis (EDAX) equipment that was coupled to the JEOL JEM-2100F TEM system.

dx.doi.org/10.1021/ac502682n | Anal. Chem. XXXX, XXX, XXX−XXX

X-ray diffraction (XRD) characterization was carried out on a Rigaku X-ray diffractometer (Rigaku Goniometer PMG-A2, CN2155D2, wavelength of λ = 0.15147 nm) with Cu Kα radiation. The specific surface area of the samples were measured with a constant volume adsorption apparatus (CHEMBET-3000) via the N_2−BET method at liquid nitrogen temperature.

All electrochemical characterizations were made on a Model 660D electrochemical workstation (CH Instruments, Austin, TX) with a single compartment, three-electrode cell at room temperatures (23 ± 2 °C). The modified electrodes, a saturated calomel electrode (SCE), and a Pt wire are used as working, reference, and auxiliary electrodes, respectively. The potential was reported vs the SCE.

RESULTS AND DISCUSSION

Characterization of AuCu Nanowires. The SEM image in Figure 1A shows the structural and morphological information of the Cu/Au sample with an equal molar ratio of Cu/Au precursors (denoted as "Cu/Au 1") taken 1 h after the reaction begins. The products are composed of highly uniform pure AuCu nanowires with an average diameter below 4.2 and 3.1 nm and length of up to 500 nm. From the image with higher magnification (Figure 1B), it can be seen that the nanowires are divided into short stems by the dotlike dark nodes. Three randomly selected typical nanowires were studied by TEM (Figures 1C−E), from which an obvious orientation, through chaining together the neighbor ends of nanodots and/or nanorods at the nodes (marked by circles) to one-dimensional nanowires, was observed. Sharp contrast can be clearly seen from TEM images of the bent nanowire. The bright and dark should be a result of the uneven distribution of the Au atoms in the wires. In this growth strategy, the Au ion has a more positive redox potential and is easier to be reduced, in comparison to that of Cu ions. Heterostructured ultrathin nanowires were thus formed by using the preformed Au nanoparticles as seeds, and the conformal overgrowth of AuCu on Au nanodots is significantly impeded by the high lattice mismatch between Au and Cu.[15] In addition, the crystal plane spacing is measured as 0.212 nm (Figure 1F), which can be ascribed to the (111) plane of face-centered cubic (fcc) Cu/Au bimetal alloys. A fast Fourier transform (FFT) pattern shows the typical polycrystalline fcc structure (Figure 1G). The lattice parameter is ∼0.38 ± 0.04 nm, which is between the lattice parameters of Cu and Au, thus the alloying nature of the nanowires can be demonstrated. A typical energy-dispersive (EDS) scanning profile captured from several positions of Figure 1A is shown in Figure 1H. This result proves that Cu/Au atoms within the nanowire are grown with almost the equal atomic ratio, which is in accord well with both the FFT and HRTEM data. Figure 1I presents the size distribution of the AuCu nanowires. The statistical diameter is ∼3.8 nm.

To explore the optimum catalytic activity, the composition and structure of the $Au_{50}Cu_{50}$ alloy nanowire has been tuned by immersing and dealloying the $Au_{50}Cu_{50}$ nanowires in a diluted HNO_3 solution. It can be seen that composition of the $Au_{50}Cu_{50}$ nanoalloy changes steadily, along with the dealloying time, and the atomic ratio of copper decreases slowly to ∼16% (Figure 2A). We guess that the remaining Cu atoms are densely enclosed by gold, which prevents any serious further corrosion of copper from the nanoalloys. Although the morphologies of the dealloyed AuCu nanomaterials remain unchanged, the changing trend in structures has been proved by the XRD data

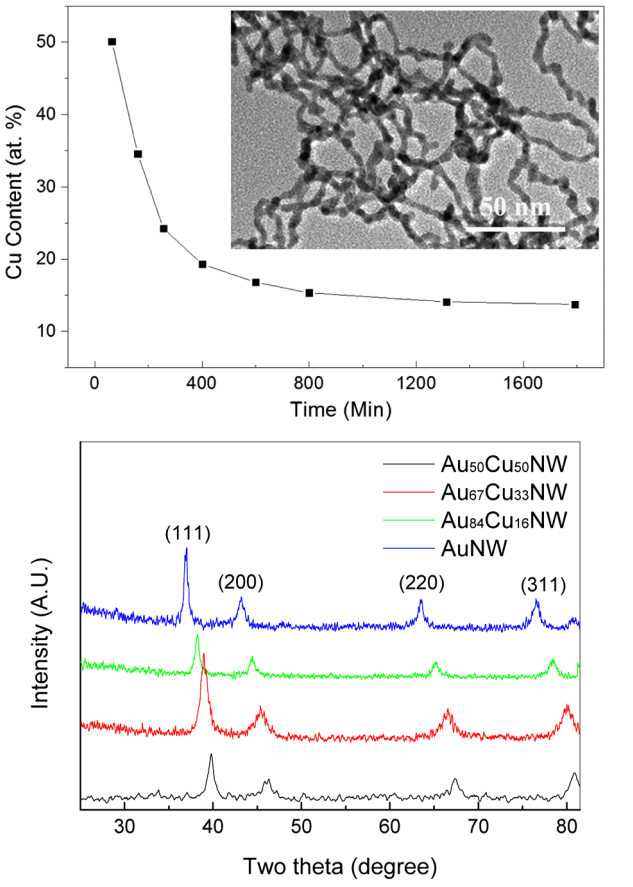

Figure 2. Typical information of the dealloyed AuCu nanowires: (A) atomic ratio of Cu in the AuCu alloy of the AuCu nanowires vs acidification time and (B) typical XRD patterns taken from samples acidified for 1, 6, and 24 h. The inset in panel (A) shows the morphology of the dealloyed AuCu nanowires, which remains almost unchanged as time varies.

(Figure 2B). As shown clearly, the (111), (200), (220), and (311) peaks shift positively, in comparison with that of Cu (JCPDS File Card No. 00-001-1241), but are shifted somewhat negatively relative to that of typical Au (JCPDS File Card No. 01-089-3697). In light of Vegard's law, the peak shift should result from the formation of an Au−Cu nanoalloy, and the crystal structure of $Au_{50}Cu_{50}$, $Au_{67}Cu_{33}$ (dealloyed for 4 h), and $Au_{84}Cu_{16}$ (dealloyed for 20 h) is the typical substitution solid solution. The lattice constants of $Au_{50}Cu_{50}$, $Au_{67}Cu_{33}$, and $Au_{84}Cu_{16}$ can be calculated as 0.376, 0.385, and 0.389 nm, correspondingly. Compared to the lattice parameters of tetragonal AuCu (a = 0.396 nm, c = 0.367 Å), the current value (a = 0.397, c = 0.370 nm) indicates the formation of intermetallic AuCu. It is also noted that the XRD peaks are somewhat broadened as the crystallite size decreases. Consistent with the Scherrer equation, the average sizes of the as-prepared AuCu nanomaterials can be calculated as 3.7 nm, which is well justified by that observed with TEM characterizations. The Au_xCu_{100-x} nanowires with different atomic ratios are used as electrocatalysts by depositing onto the electrode surface. Porous nature of the nanowire layer on the electrode surface can be proved by SEM images shown in Figure S1 in the Supporting Information (SI). Such three-dimensionally entangled nanochains provide both a tight bond to the electrode surface and abundant adsorbing sites for the collecting and detection of the analyte. The diffusion and

dx.doi.org/10.1021/ac502682n | Anal. Chem. XXXX, XXX, XXX−XXX

adsorption/desorption of the analyte is significantly promoted, and the electron transport at the interface is sharply facilitated in the sensing layer.

Electrocatalytic Activity toward the Oxidation of H_2O_2. To investigate the catalytic activity on the oxidation of H_2O_2, the Au_xCu_{100-x} nanowires were co-immobilized onto a GCE, as reported previously.[16] For comparison, Au nanowire-modified electrodes (referenced hereafter as AuNWE) were also fabricated with the same immobilization mass and procedure. For convenience, all the peak currents are normalized to the electrochemical active surface, so that the electrocatalytic activity for H_2O_2 oxidation can be compared directly. Here, analogous voltammograms with similar symmetrical characteristics have been disclosed from all three electrodes, and much higher current densities are observed on the Au_xCu_{100-x} nanowire-modified electrodes (Au_xCu_{100-x}NWEs; see Figure 3). The current densities on

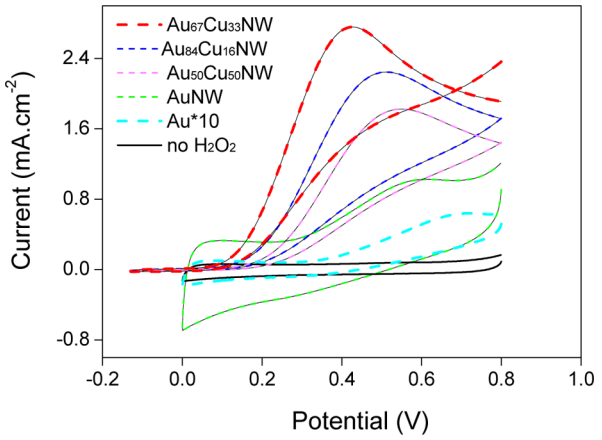

Figure 3. Cyclic voltammograms (CVs) of the Au_xCu_{100-x}NWE electrodes and the AuNWEs in N_2-saturated 0.1 M phosphate buffered saline (PBS) solution containing 5 mM H_2O_2 at a scan rate of 50 mV s^{-1}.

the Au_xCu_{100-x}NWE electrodes are more than 10 times higher than that of the Au and Cu electrodes. Analogously, the effect of the dealloying process on the electrocatalytic activity of Au_xCu_{100-x} electrodes also has been studied. The $Au_{67}Cu_{33}$NWE electrode shows the highest specific electrocatalytic activity, with an enhancement factor of up to 20, although the $Au_{84}Cu_{16}$ catalyst provides the highest electrode active surface area (see Figure S2 in the SI). Thus, it may be concluded that both the electron coupling and the large specific surface area enhance the electrocatalytic activity significantly, and the change in atomic environment of the dealloyed Au_xCu_{100-x} nanowires also make a definite contribution. In this sense, there is an optimum atomic ratio of the Au_xCu_{100-x} nanowires for the oxidation of H_2O_2. Considering that the dealloying process generally enlarges the specific surface area of $Au_{84}Cu_{16}$, the greatly enhanced oxidation currents (30%, normalized to the total mass of Au and Cu) of $Au_{67}Cu_{33}$ should not be so much a result of additional Cu weight as that of synergetic effects among the Cu−Au atoms. On the one hand, both Cu and Au have excellent electronic conductivity, and the latter is well-known for its sound catalytic activity. On the other hand, the dissolution of copper from the Au_xCu_{100-x} nanowires also enlarges the pore volume and provides abundant active sites.[17] In this strategy, the alloyed Au atoms show the specific electrocatalytic activity and long-term stability, while the alloyed copper promotes the formation of Cu−OR transition states. It is well-known that copper also is a good electron donator, which helps to increase the electric conductivity and intensify the electron coupling. Furthermore, the existence of Cu atoms reduces the binding energy of the Au 4f orbital electron and therefore the Au−RO bonding interaction. As a consequence, the strong interaction among the Cu and Au electron cloud within the Au_xCu_{100-x} nanowires results in a synergetic effect, which contributes to the fast renewing of clean gold spots for H_2O_2 oxidation and enhances the long-term catalytic performance.[7a,18]

Because of the fact that the highest electrochemical activity for oxidation of H_2O_2 is observed on the $Au_{67}Cu_{33}$NWE electrode, application of the as-prepared bimetal nanomaterial with the above-mentioned atomic ratio for detection of H_2O_2 was intensively studied in this work. Real-time amperometric detection of H_2O_2 was carried out by successive injection of H_2O_2 into 0.1 mM phosphate buffered saline (PBS) solution under constant stirring at 0.484 V. (See Figure 4.) After the

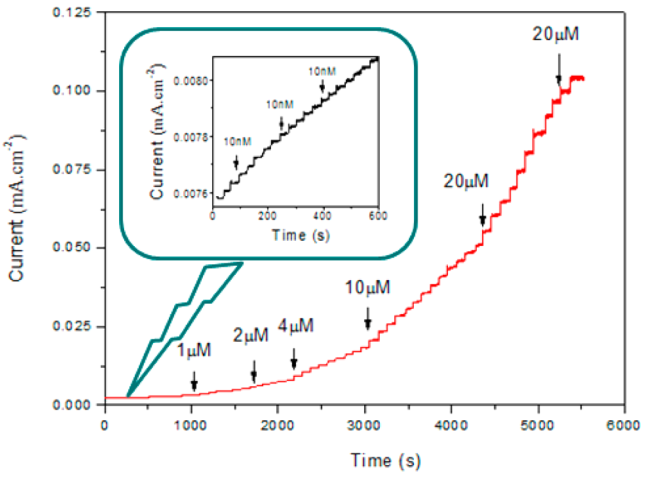

Figure 4. Amperometric responses of the AuCuNWE electrode to the successive addition of H_2O_2 in the N_2-saturated 0.1 M PBS at 0.484 V. The inset shows a close look of the response current to 10 nM H_2O_2.

addition of H_2O_2, the steady-state current can be achieved within 3 s, and current peak appears even in the presence of trace amounts of H_2O_2 (nanomolars), indicating a very quick and acute response (see Figure 5). This sensitivity to H_2O_2 at the nanomolar level is really uncommon for such an inorganic

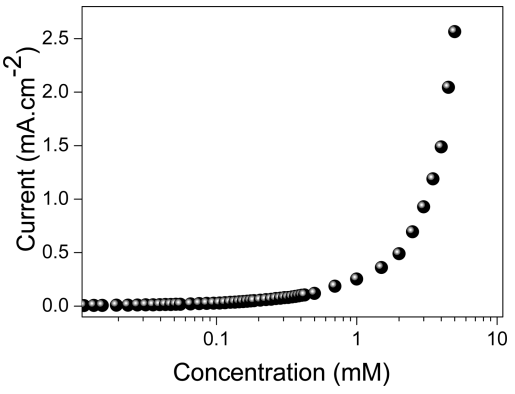

Figure 5. Current response of the electrode, relative to the logarithm of the H_2O_2 concentration.

dx.doi.org/10.1021/ac502682n | Anal. Chem. XXXX, XXX, XXX−XXX

nanomaterial-based electrode, suggesting its wide catalytic/sensing applications to biosystems that contain H_2O_2 with different concentrations. In the linear range from 3.0 nM to 360 nM, the sensitivity is 2.71×10^3 mA cm^{-2} M^{-1} (Figure 6A). In the linear range from 360 nM to 440 μM, the sensitivity is 285 mA cm^{-2} M^{-1} (Figure 6B). The detection limit (2.0 nM) is satisfactory in comparison with the reported H_2O_2 sensors (Figure 7).[19] A concise comparison has been made and is shown in Table 1, which indicates a bright future of the Au_xCu_{100-x} nanowires for electrochemical sensors. Besides the above-mentioned advantages of Au_xCu_{100-x} nanowires, the excellent sensing performance may also partly attribute to the highly porous nature of the nanowire layer. At the electrode surface, the well-dispersed targeting molecules can diffuse freely within the large pores and be fully adsorbed and collected, while frequent collision among concentrated H_2O_2 molecules may result in strong interactions, which hinders their sensitive detection.[4b]

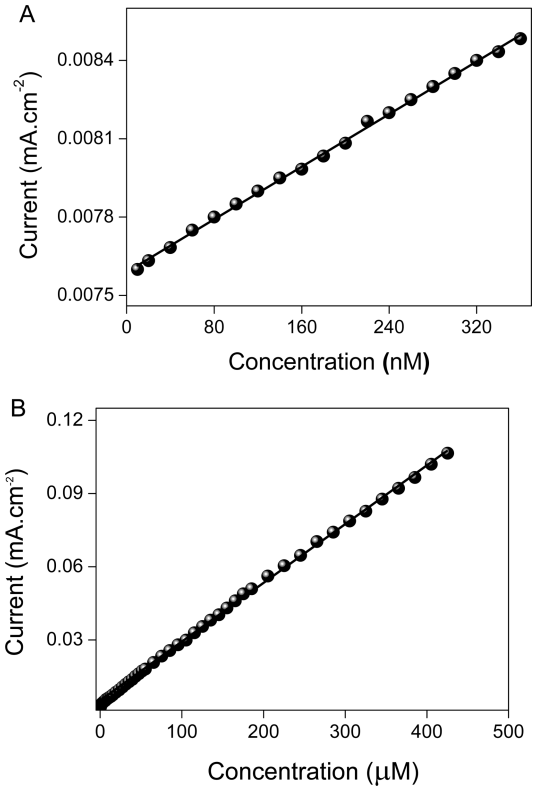

Figure 6. (A) Calibration curve of the amperometric response to the concentration of H_2O_2 from 5.0 nM to 360 nM. (B) Calibration curve of the amperometric response to the concentration of H_2O_2 from 360 nM to 440 μM.

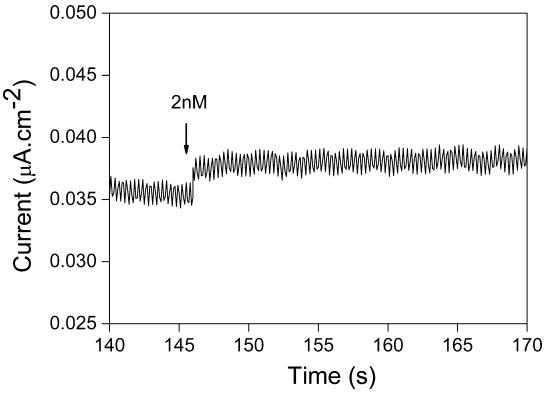

Figure 7. Determination limit of the AuCuNWE electrode.

Table 1. Comparison of Different Measurements for H_2O_2 determination

electrode material	reference	linear range	detection limit (μM)
Prussian Blue	21	up to 100 mM	0.01
MoS_2	1a	up to 0.1 mM	0.0025
Fe_3O_4	22	up to 0.1 mM	3
myoglobin	11a	up to 1.4 mM	0.5
SiO_2–cellulose	2c	NA	1
yellow fluorescent protein	4b	NA	0.1
$Au_{67}Cu_{33}$ nanowire	this work	up to 0.4 mM	0.002

Another important issue for a biosensor is the capability to distinguish the targeting molecular from the interferents normally present in an alkaline environment. To examine the anti-interference response, the AuCuNWE electrode was tested by succession injection of 0.1 mM H_2O_2 and 0.1 mM of interfering materials into a 0.1 M PBS solution at 0.484 V (vs SCE). It can be observed that, after the injection of 0.1 mM H_2O_2, the current apparently increases, while no distinctive current change can be observed after the injection of 0.1 mM of ascorbic acid (AA), uric acid (UA), and dopamine (DA) (see Figure 8); thus, a good selectivity has been demonstrated. CV tests also confirm this sound selective catalysis (See Figure S3 in the SI.)

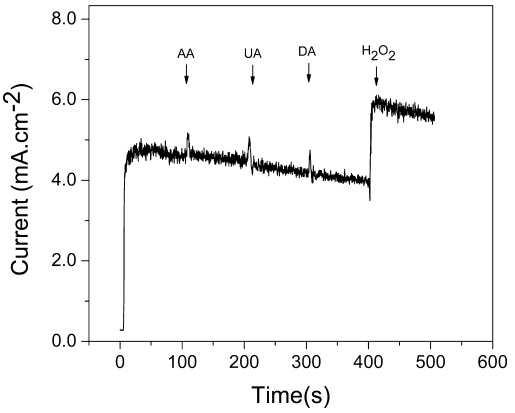

Figure 8. Chronoamperometric curves of the AuCuNWE electrode in a 0.1 M phosphate buffer (pH 7.4) with the successive addition of 0.1 mM ascorbic acid (AA), 0.1 mM uric acid (UA), 0.1 mM dopamine (DA), and 0.1 mM H_2O_2 with a constant potential at 0.484 V.

Real-time performance monitoring of the as-fabricated electrode has also been checked by detecting H_2O_2 released from the Raw 264.7 cell. 3-[(3-Cholamidopropyl) dimethylammonio]-1-propanesulfonate (CHAPS) was selected as a stimulant for the cell to exude H_2O_2. Here, $\sim 2 \times 10^6$ cells were suspended into PBS solution (20 mL). After the addition of 0.3 μM CHAPS, ~20 nM H_2O_2 was released, and the current obviously changes. Meanwhile, no obvious current response can be seen without the treatment of CHAPS or in the absence of the Raw 264.7 cell (see Figure 9). Figure S4 in the SI shows a typical amperometric response of the $Au_{67}Cu_{33}$NWE

dx.doi.org/10.1021/ac502682n | Anal. Chem. XXXX, XXX, XXX–XXX

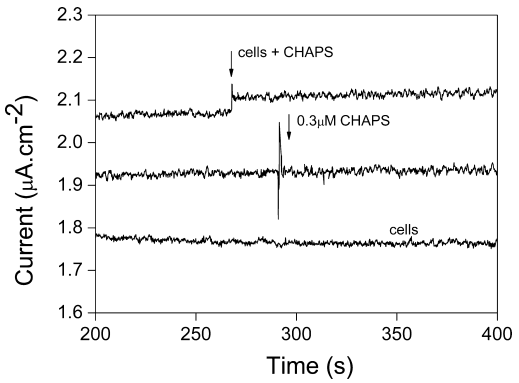

Figure 9. Amperometric responses of the AuCuNWE electrode to the addition of 0.3 μM CHAPS with and without Raw 264.7 cells, as well as in the presence of Raw 264.7 cells without CHAPS in the N_2-saturated 0.1 M PBS at 0.484 V.

electrode to 0.3 μM CHAPS in the presence of both Raw 264.7 cells and catalase. The current intensity increases distinctively, and the linear dependency is analogous to that observed from PBS solutions of H_2O_2 added directly. Thus, it can be deduced that the strong current signals in Figure 9 are caused by H_2O_2 released from the Raw 264.7 cell, considering that catalase can selectively decomposes H_2O_2. The H_2O_2 amount released by the raw 264.7 cells has also been measured with the fluorescence methods, which agreed well with the present electrochemical method and demonstrated the accuracy of the AuCuNW catalyst-based electrochemical sensor.[20] The recovery of the as-fabricated H_2O_2 sensor falls into the range of 84%−112% if 20−50 nM of H_2O_2 was spiked into the cell sample. Furthermore, Figure S5 in the SI shows repeatable current signals, indicating that the performance is reliable and convincing.

Reproducibility of the AuCuNWE electrodes has been evaluated by preparing five parallel electrodes for the determination of 5 mM H_2O_2. The relative standard deviations (RSDs) of the five electrodes are 3.12% for one test (Figure S6 in the SI) and 3.8% for 100 successive measurements (Figure S7 in the SI). This RSD is rather good, as far as the reproducibility and precision are concerned. After being kept at ambient temperature for 2 weeks, repeatable sensing performance can also been presented by the electrode for determination of H_2O_2 analyte, demonstrating satisfactory chemical and structural stability of the film.

CONCLUSION

In summary, a simple wet chemical route has been successfully developed for the facile preparation of AuCu nanowires. Compositions of the bimetallic nanowire are then tuned by leaching Cu atoms from the AuCu nanomaterials with acid solution. Because of the large surface and strong electron coupling, excellent electrocatalytic activity has been demonstrated. Nonenzymatic H_2O_2 biosensors with high sensitivity and selectivity are thus fabricated by using the AuCu nanowire as modifying layers. Interestingly, a very low detection limit for H_2O_2 is also shown (~2 nM), which is sensitive enough for practical applications such as detecting H_2O_2 that has been released by living cells. It can thus be concluded that the three dimensionally interconnected nanoalloys help to increase the pore volume/surface and structural stability, while the dealloying process is powerful in preparing bimetal nanocatalysts with enhanced electrocatalytic activity.

ASSOCIATED CONTENT

Supporting Information

This material is available free of charge via the Internet at http://pubs.acs.org.

AUTHOR INFORMATION

Corresponding Author

*E-mail: caoxia12@pku.edu.cn.

Notes

The authors declare no competing financial interest.

ACKNOWLEDGMENTS

We thank the financial support from the National Natural Science Foundation of China (NSFC no. 21173017, 51272011, and 21275102), the Program for New Century Excellent Talents in University (NWET-12-0610), The science and technology research projects from education ministry (213002A), National "Twelfth Five-Year" Plan for Science & Technology Support (No. 2013BAK12B06), Project of Thousand Talents of Chinese High-leveled Talents and the Knowledge Innovation Program of the Chinese Academy of Science (Grant No. KJCX2-YW-M13).

REFERENCES

(1) (a) Wang, T. Y.; Zhu, H. C.; Zhuo, J. Q.; Zhu, Z. W.; Papakonstantinou, P.; Lubarsky, G.; Lin, J.; Li, M. X. *Anal. Chem.* **2013**, *85* (21), 10289−10295. (b) Shandost-fard, F.; Salimi, A.; Khezrian, S. *Biosens. Bioelectron.* **2014**, *53*, 355−362.

(2) (a) Suarez, G.; Santschi, C.; Martin, O. J. F.; Slaveykova, V. I. *Biosens. Bioelectron.* **2013**, *42*, 385−390. (b) Lou, Z. R.; Li, P.; Sun, X. F.; Yang, S. Q.; Wang, B. S.; Han, K. L. *Chem. Commun.* **2013**, *49* (4), 391−393. (c) Jiang, Y. J.; Wang, W.; Li, X. T.; Wang, X. C.; Zhou, J. W.; Mu, X. D. *ACS Appl. Mater. Interfaces* **2013**, *5* (6), 1913−1916.

(3) (a) Jin, H.; Heller, D. A.; Kalbacova, M.; Kim, J. H.; Zhang, J. Q.; Boghossian, A. A.; Maheshri, N.; Strano, M. S. *Nat. Nanotechnol.* **2010**, *5* (4), 302−309. (b) Zhang, Y.; Wu, C. Y.; Zhou, X. J.; Wu, X. C.; Yang, Y. Q.; Wu, H. X.; Guo, S. W.; Zhang, J. Y. *Nanoscale* **2013**, *5* (5), 1816−1819.

(4) (a) Kim, J. H.; Patra, C. R.; Arkalgud, J. R.; Boghossian, A. A.; Zhang, J. Q.; Han, J. H.; Reuel, N. F.; Ahn, J. H.; Mukhopadhyay, D.; Strano, M. S. *ACS Nano* **2011**, *5* (10), 7848−7857. (b) Tsourkas, A.; Newton, G.; Perez, J. M.; Basilion, J. P.; Weissleder, R. *Anal. Chem.* **2005**, *77* (9), 2862−2867.

(5) Xu, C.; Ren, J. S.; Feng, L. Y.; Qu, X. G. *Chem. Commun.* **2012**, *48* (31), 3739−3741.

(6) Bhattacharjee, S.; Jiang, J. J.; Chatterjee, S.; Deterding, L.; Sinha, B.; Mason, R. *Free Radical Biol. Med.* **2012**, *53*, S133−S133.

(7) (a) Wang, J. J.; Han, D. X.; Wang, X. H.; Qi, B.; Zhao, M. S. *Biosens. Bioelectron.* **2012**, *36* (1), 18−21. (b) Sun, X. L.; Guo, S. J.; Liu, Y.; Sun, S. H. *Nano Lett.* **2012**, *12* (9), 4859−4863. (c) Chen, L.; Wang, X. J.; Zhang, X. T.; Zhang, H. M. *J. Mater. Chem.* **2012**, *22* (41), 22090−22096. (d) Liu, Y.; Hu, N. F. *Biosens. Bioelectron.* **2009**, *25* (1), 185−190.

(8) Saurin, A. T.; Eaton, P. *J. Mol. Cell Cardiol.* **2004**, *37* (1), 249−249.

(9) (a) Meng, X. W.; Wei, J. F.; Ren, X. L.; Ren, J.; Tang, F. Q. *Biosens. Bioelectron.* **2013**, *47*, 402−407. (b) Li, W. Z.; Kuai, L.; Qin, Q.; Geng, B. Y. *J. Mater. Chem. A* **2013**, *1* (24), 7111−7117. (c) Chen, K. J.; Pillai, K. C.; Rick, J.; Pan, C. J.; Wang, S. H.; Liu, C. C.; Hwang, B. J. *Biosens. Bioelectron.* **2012**, *33* (1), 120−127.

(10) Chakraborty, S.; Raj, C. R. *Biosens. Bioelectron.* **2009**, *24* (11), 3264−3268.

(11) (a) Xia, P. P.; Liu, H. Q.; Tian, Y. *Biosens. Bioelectron.* **2009**, *24* (8), 2470−2474. (b) Miah, R.; Ohsaka, T. *Anal. Chem.* **2006**, *78* (4), 1200−1205. (c) Luo, Y. P.; Liu, H. Q.; Rui, Q.; Tian, Y. *Anal. Chem.* **2009**, *81* (8), 3035−3041. (d) Karam, P.; Halaoui, L. I. *Anal. Chem.* **2008**, *80* (14), 5441−5448. (e) Niu, X. H.; Chen, C.; Zhao, H. L.; Chai, Y.; Lan, M. B. *Biosens. Bioelectron.* **2012**, *36* (1), 262−266. (f) Curulli, A.; Valentini, F.; Orlanduci, S.; Terranova, M. L.; Palleschi, G. *Biosens. Bioelectron.* **2004**, *20* (6), 1223−1232. (g) Zhang, H. J.; Watanabe, T.; Okumura, M.; Haruta, M.; Toshima, N. *Nat. Mater.* **2012**, *11* (1), 49−52. (h) Zhang, L. F.; Zhong, S. L.; Xu, A. W. *Angew. Chem., Int. Ed.* **2013**, *52* (2), 645−649. (i) Powers, D. C.; Ritter, T. *Nat. Chem.* **2009**, *1* (5), 419. (j) Huang, X. Q.; Tang, S. H.; Mu, X. L.; Dai, Y.; Chen, G. X.; Zhou, Z. Y.; Ruan, F. X.; Yang, Z. L.; Zheng, N. F. *Nat. Nanotechnol.* **2011**, *6* (1), 28−32.

(12) (a) Nagaiah, T. C.; Schafer, D.; Schuhmann, W.; Dimcheva, N. *Anal. Chem.* **2013**, *85* (16), 7897−7903. (b) Taduri, B. P.; Abu Sohel, S. M.; Cheng, H. M.; Lin, G. Y.; Liu, R. S. *Chem. Commun.* **2007**, *24*, 2530−2532. (c) Tang, Y.; Xu, S. D.; Dai, Y. H.; Yan, X. Q.; Li, R. H.; Xiao, L. P.; Fan, J. *Chem. Commun.* **2014**, *50* (2), 213−215. (d) Wang, X. H.; Dong, S. L.; Yao, Z. L.; Feng, L.; Daka, P.; Wang, H.; Xu, Z. H. *Org. Lett.* **2014**, *16* (1), 22−25. (e) Zeng, J.; Zhang, Q.; Chen, J. Y.; Xia, Y. N. *Nano Lett.* **2010**, *10* (1), 30−35.

(13) (a) Cao, X.; Wang, N.; Jia, S.; Shao, Y. H. *Anal. Chem.* **2013**, *85* (10), 5040−5046. (b) Cao, X.; Wang, N.; Jia, S.; Guo, L.; Li, K. *Biosens. Bioelectron.* **2013**, *39* (1), 226−230. (c) Cao, X.; Han, Y.; Gao, C. Z.; Huang, X. M.; Xu, Y.; Wang, N. *J. Mater. Chem. A* **2013**, *1* (47), 14904−14909.

(14) Kung, C. C.; Lin, P. Y.; Buse, F. J.; Xue, Y. H.; Yu, X.; Dai, L. M.; Liu, C. C. *Biosens. Bioelectron.* **2014**, *52*, 1−7.

(15) Yuan, Q.; Zhou, Z. Y.; Zhuang, J.; Wang, X. *Chem. Mater.* **2010**, *22* (7), 2395−2402.

(16) Dudin, P. V.; Snowden, M. E.; Macpherson, J. V.; Unwin, P. R. *ACS Nano* **2011**, *5* (12), 10017−10025.

(17) Pavanello, M.; Auerbach, D. J.; Wodtke, A. M.; Blanco-Rey, M.; Alducin, M.; Kroes, G. J. *J. Phys. Chem. Lett.* **2013**, *4* (21), 3735−3740.

(18) Chen, K.; Strasser, C. E.; Schmitt, J. C.; Shearer, J.; Catalano, V. J. *Inorg. Chem.* **2012**, *51* (3), 1207−1209.

(19) (a) Liu, Y. X.; Dong, X. C.; Chen, P. *Chem. Soc. Rev.* **2012**, *41* (6), 2283−2307. (b) Shao, Y. Y.; Wang, J.; Wu, H.; Liu, J.; Aksay, I. A.; Lin, Y. H. *Electroanalysis* **2010**, *22* (10), 1027−1036. (c) Chen, D.; Feng, H. B.; Li, J. H. *Chem. Rev.* **2012**, *112* (11), 6027−6053.

(20) Kim, G.; Lee, Y.-E. K.; Xu, H.; Philbert, M. A.; Kopelman, R. *Anal. Chem.* **2010**, *82*, 2165−2169.

(21) Karyakin, A. A.; Puganova, E. A.; Budashov, I. A.; Kurochkin, I. N.; Karyakina, E. E.; Levchenko, V. A.; Matveyenko, V. N.; Varfolomeyev, S. D. *Anal. Chem.* **2004**, *76* (2), 474−478.

(22) Wei, H.; Wang, E. *Anal. Chem.* **2008**, *80* (6), 2250−2254.